Colloid Polym Sci (2005) 283: 905–916
DOI 10.1007/s00396-004-1238-5

ORIGINAL CONTRIBUTIONS

Oliver Lade
Carlos C. Co
Patricia Cotts
Reinhard Strey
Eric W. Kaler

Microemulsion polymerization: phase behavior driven mechanistic changes

Received: 2 July 2004
Accepted: 5 November 2004
Published online: 2 February 2005

O. Lade · R. Strey (✉)
Institut für Physikalische Chemie, Universität zu Köln, Luxemburger Str. 116, Köln, 50939, Germany
E-mail: rstrey@uni-koeln.de
Tel.: +49-221-4704458
Fax: +49-221-4705104

C. C. Co · E. W. Kaler
Center for Molecular and Engineering Thermodynamics, Department of Chemical Engineering, University of Delaware, Newark, DE 19716, USA

P. Cotts
DuPont Company, Central Research and Development, Wilmington, DE 19880, USA

Present address: O. Lade
Siemens AG, Industriepark Höchst, G811, Frankfurt, 65926, Germany

Present address: C. C. Co
Department of Chemical Engineering, University of Cincinnati, Cincinnati, OH 45230, USA

Abstract We have examined the phase behavior of anionic microemulsions of the general type water/NaCl–hexyl methacrylate (C_6MA)-bis(2-ethylhexyl)sulfosuccinate (AOT)/sodium dodecyl sulfate (SDS) with respect to temperature and composition. Monomer partitioning measurements and kinetic experiments show good agreement with the Morgan model (de Vries et al. in Macromolecules 34:3233, 2001) for droplet-type microemulsions that do not phase separate as monomer is consumed. In contrast, balanced microemulsions, which efficiently solubilize large amounts of monomer, exhibit dramatic effects on the polymerization kinetics as the phase behavior changes. Our findings suggest that the appearance of a liquid crystalline mesophase in the binary water–surfactant system of the respective microemulsion causes a phase separation during polymerization and, thus, a severe deviation from previous mechanistic models.

Keywords Microemulsion polymerization · Kinetics · Mechanism · Ionic surfactant · Phase behavior · Alkyl methacrylate · Phase inversion temperature · Emulsification-failure boundary

Introduction

Emulsion polymerization is a widely used process for the preparation of polymer latexes with a large variety of practical and specialized applications from common household paints to specially modified ferromagnetic and fluorescent latexes for biological assays. Typical latexes prepared via emulsion polymerization are limited to sizes >100 nm that are too large for some sensory and penetrant-probe applications wherein maximum surface area and minimum particle size are desirable. For these applications and others requiring high molecular weight polymer, nanometer-sized latex particles prepared via free radical microemulsion polymerization [2–4] are useful. Such particles often contain only one polymer chain with molecular weight exceeding 10^7 Da. Although the first reports of polymerizable microemulsions date back more than 20 years, it has

only been recently that a reliable mechanistic picture has been formulated from the large variety of available studies that often suggest different and conflicting mechanistic interpretations.

From extensive phase behavior, microstructure, kinetic, particle size and molecular weight distributions (MWD), and monomer partitioning investigations of microemulsion polymerization of the quasi-ternary system H_2O–monomer–dodecyltrimetylammonium bromide/didodecyldimetylammonium bromide (DTAB/DDAB) [1, 5–11], a quantitative model has been derived and validated. Previously, microemulsion compositions were chosen with the objective of systematically probing the mechanisms of polymerization with minimal effort exerted to locate efficient microemulsions containing high ratios of monomer to surfactant for polymerization. In this study, we focus on a combination of anionic surfactants [bis(2-ethylhexyl)sulfosuccinate (AOT) and sodium dodecyl sulfate (SDS)] with a modicum of salt (NaCl) that was expected to yield efficient polymerizable microemulsions requiring only low ratios of surfactant to monomer. With the model of Morgan et al. [8, 9, 11] as a theoretical framework for comparison with experimental results, we will validate the assumptions underlying the model for anionic microemulsions and point out certain cases and reasons for failure. While the previous investigations largely avoided regions of complex phase behavior and demonstrated only the effects of approaching the emulsification-failure boundary on monomer partitioning, we focus here on the polymerization of efficient microemulsions near the balanced state and demonstrate the dramatic influence phase behavior can have on polymerization characteristics.

Following our previous report [12] of polymerizable non-ionic microemulsions, we applied the same procedures for determining the balanced state of zero mean curvature (phase inversion) and one-phase microemulsions regions for polymerization. Two phase diagrams are recorded as a function of temperature while varying one composition variable. In one diagram, often referred to as a fish diagram due to its characteristic shape, the surfactant overall weight fraction is varied in mixtures containing equal volumes of water and monomer. In the other diagram, the phase behavior is recorded while adding monomer to a binary mixture of water and surfactant (Fig. 1).

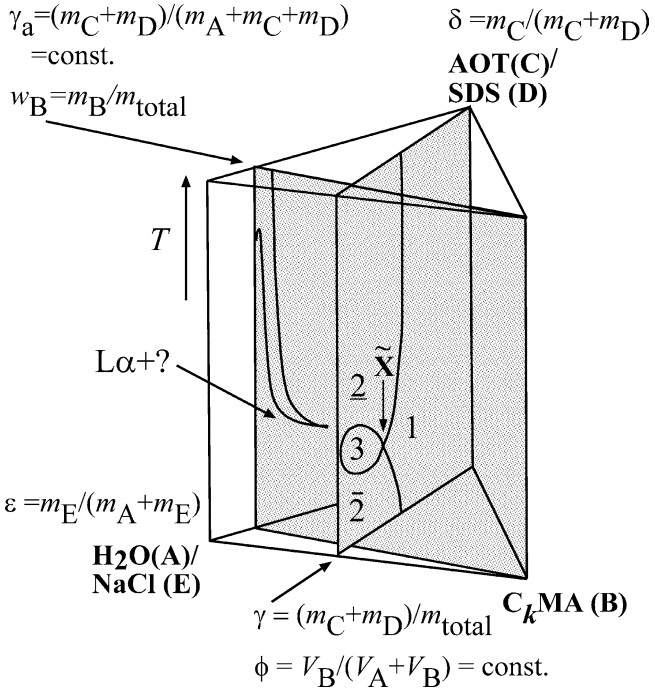

Fig. 1 Characteristic sections through the phase prism applied for phase behavior investigations (one-phase microemulsion channel and fish diagram). Definitions of parameters for pseudo-ternary systems are given as well. Ideal mixture is assumed so that a constant weight ratio of the components also means a constant volume ratio

The mechanistic model for free radical microemulsion polymerization

The polymerization of microemulsions consisting of nanometer-sized surfactant micelles swollen with monomer typically starts from the formation of aqueous free radicals generated by thermal decomposition of the initiator. These aqueous free radicals continuously enter and initiate polymerization within the monomer swollen-micelles through the reaction. Monomer in uninitiated micelles continuously diffuses through the aqueous phase to the polymerization sites within the initiated micelles transforming them into larger polymer particles. However, even after complete polymerization, only a very small fraction (approximately 1 in 1,000) of the initial monomer swollen-micelles are transformed into polymer particles. Rapid transport of monomer between micelles and polymer particles throughout the reaction assures thermodynamic control of monomer partitioning.

The original kinetic model by Morgan et al. [8] for free radical polymerization in microemulsions is based on the following assumptions, the validity of which must be carefully considered on a case to case basis:

a. There is a constant rate of radical generation from initiator decomposition ρ_0—the half-life of the V50 initiator we use is approximately 10 h at 60 °C and much longer than the total reaction times.
b. There is apparently negligible biradical termination due to the large number of monomer-swollen micelles relative to polymer particles, of which only a very small fraction host a polymer with a growing radical

end. The probability of an aqueous radical locating and terminating with a radical containing particle is thus minimal and the number of radicals present N^* is given solely by the rate of radical generation ρ_0. Further theoretical and experimental analysis of this assumption for a variety of monomers [1] shows that this approximation is valid for hexyl methacrylate (C_6MA) polymerizations especially at low initiator concentrations and low conversions, but not necessarily so for less hydrophobic and/or less reactive monomers, such as MMA or styrene. The higher water-solubility and/or lower propagation rate constants extends the time period prior to propagation during which radical derivatives of these monomers are capable of diffusing through micelles and particles across the aqueous phase, thus increasing the probability of terminating with a radical containing particle. The almost "living" character of certain free-radical polymerizations in microemulsions is brought about by the high degree of compartmentalization in these systems that could potentially be degraded by microstructural changes over the course of polymerizations as demonstrated in this work.

c. Chain propagation ceases due to radical transfer to either monomer or surfactant. If either event is unlikely, ultra-high molecular weight polymers are formed. The diffusion of monomer in these nanometer-sized particles is sufficiently fast such that even hydrophobic C_6MA monomer radicals generated by chain transfer, exit to initiate polymerization in another swollen-micelle. The latex particles formed are thus composed of single polymer chains and the number of particles is much larger than the total number of initiator generated radicals.

d. The concentration of monomer at the locus of polymerization in the polymer particles decreases linearly with overall conversion f. SANS studies of monomer partitioning between polymer particles and swollen-micelles confirm that this approximation is adequate for a wide range of C_6MA, n-C_4MA, t-C_4MA, and styrene microemulsion polymerizations with DTAB surfactant. Theory and experiments show that when the monomer loading of the original microemulsion is progressively reduced relative to the maximum concentration set by the emulsification-failure phase boundary, increasingly non-linear monomer concentration profiles result [5]. However, an additional complication which has not been considered is that the phase diagram of numerous monomer/water/surfactant systems exhibit narrow one-phase microemulsion regions bounded by both *maximum* and *minimum* loadings of monomer. In this work, we explore the polymerization of these microemulsions wherein highly non-linear variations in monomer chemical potential are anticipated over the course of polymerization.

With these approximations, the rate of polymerization as a function of time t and conversion can be calculated as follows:

$$\frac{\mathrm{d}f}{\mathrm{d}t} = At\mathrm{e}^{-\frac{1}{2}At^2} = (1-f)\sqrt{-2A\ln(1-f)} \tag{1}$$

wherein A is a bundle of constants:

$$A = \frac{k_\mathrm{p} C_0 \rho_0}{M_0}, \tag{2}$$

k_p is the propagation rate constant, C_0 is the initial concentration of monomer at the locus of polymerization, ρ_0 is the rate of radical generation and M_0 is the initial overall concentration of monomer in the microemulsion.

From the derivative of Eq. 1 the time and conversion at which the maximum polymerization rate occurs are:

$$\bar{t} = \sqrt{\frac{1}{A}} \tag{3}$$

and

$$\bar{f} = 0.39 \tag{4}$$

Kaler et al. have shown that this model yields quantitative predictions for C_6MA microemulsion polymerizations with certain cationic surfactants. For other monomers, however, the maximum rate can shift to conversions as low as 20% due to non-linearities in monomer concentration profiles, glass transition effects, and non-negligible biradical termination during the reaction.

Phase behavior and interfacial curvatures of ionic microemulsions

Microemulsions are transparent, thermodynamically stable phases of water and oil domains microscopically separated by a monolayer of surfactant that we refer to as the interfacial film. Microemulsions can exist independently as single phases or coexist with excess water, oil, and/or a lamellar Lα phase composed of planar surfactant monolayers separating water and oil subdomains. The phase behavior of ionic surfactants has not been studied to the same extent as non-ionic surfactants and reliable knowledge of the general patterns of ionic microemulsion phase behavior is limited largely to sodium AOT.

The curvature of the interfacial film

The interfacial curvature of the surfactant film is the primary determinant of surfactant self-assembly and

microemulsion phase behavior and microstructure. Interfacial curvatures in microemulsions can vary over several orders of magnitude including both signs, with empty micelles and empty inverse micelles marking the two extremes [13]. By changing the curvature from positive (toward oil) to negative (toward water) one can form oil–water and water–oil microemulsions. At the balanced state of zero mean curvature, where the system undergoes a phase inversion, water and oil can be co-solubilized most efficiently with a minimum of surfactant [14–17]. The preferred microstructure at the balanced state is either a bicontinuous sponge-like or lamellar [18–22]. Experimental findings show that the lamellar microstructure is preferred for high surfactant-to-oil-ratios and rigid interfacial films. However, even when the one-phase lamellar region is small, the two-phase coexistence of the lamellar phase with either a microemulsion or an excess oil or water phase typically dominates the phase prism at near zero mean curvature states. As we will show later, consumption of monomer over the course of polymerization of an initially one-phase balanced microemulsion can increase the effective surfactant-to-oil ratio resulting in the simultaneous coexistence of microemulsion and lamellar phases with the polymer latexes.

Finding the balanced state of zero mean curvature in ionic microemulsions

As Kahlweit and Strey [23] have pointed out, the most rewarding experimental method for finding the balanced state is to record the so-called fish diagram, i.e., the phase transition temperatures of mixtures with a varying overall surfactant weight fraction γ while keeping all other composition variables constant with the oil/(oil + water) volume ratio fixed at $\phi = 0.5$. At a certain phase inversion temperature $\tilde{T}$ one finds the least weight fraction of surfactant $\tilde{\gamma}$ necessary to form a one-phase bicontinuous microemulsion by extrapolating the two phase boundaries where the one-phase microemulsion turns two-phase toward higher and lower temperatures. The $\tilde{X}$ or fish tail point marks the intersection of the one- and three-phase region and is the most important characteristic for the efficiency of the surfactant and for the properties that lead to a phase inversion (Fig. 1).

Choosing appropriate microemulsifying surfactants for efficient balanced microemulsions is more challenging for ionic surfactants. Compared to non-ionic C_iE_j surfactants whose phase behavior has been exhaustively studied, the hydrophilic moiety of ionic surfactants cannot be changed gradually. Single-tail ionic surfactants are often much too hydrophilic, i.e., they induce a high curvature, yielding inefficient microemulsions with most oils. Balancing the surfactant by enlargement of the lipophilic tail, though, is not practical, as such surfactants typically have high Krafft temperatures and phase diagrams that are dominated by single- or two-phase lamellar regions. In the present work, we describe a strategy for formulating microemulsions with double-tailed dioctylsulfosuccinate surfactant (AOT) by utilizing the single-tailed surfactant, SDS to suppress lamellar phases, and salt to balance the curvature of the interfacial film.

From pertinent literature [24, 25] on AOT fish diagrams we observe the following trends. (a) For ternary microemulsion of the type water–alkane–AOT the $\tilde{X}$ point lies slightly below the melting point of those mixtures and the lamellar phase is predominant. Small amounts of salt must be added to record the entire fish diagram. Here, we will express the salinity in terms of the weight fraction ε of salt with respect to all hydrophilic components of the microemulsions. A slight increase in ε of just 0.1% can cause an enormous increase in $\tilde{T}$ of about 5–20 K. With increasing salinity, the efficiency also decreases and the lamellar phase is partly suppressed. (b) Microemulsions containing more hydrophobic oils require higher salinity to reach the balanced state. For highly purified AOT surfactant typical salinities at $\tilde{T} = 32\,^{\circ}\mathrm{C}$ would be $\varepsilon = 0.008$ (0.8%) for octane and $\varepsilon = 0.004$ (0.4%) for isooctane. (c) At constant salinity the balanced state for more hydrophobic oils lies at lower temperatures. (d) In contrast to non-ionic microemulsions the fish is slightly tilted to higher temperatures. This phenomena is a consequence of the concomitant increase of counterions in the water domains as one increases the surfactant concentration. (e) Different grades of AOT purity have severe effects on the phase behavior due to its strong dependence on salinity and ionic impurities.

Water-rich microemulsions for polymerization

Defining the overall weight fraction of C_kMA in the microemulsion as $w_B = m_{C_kMA}/m_{total}$, a phase diagram representing a vertical $w_B(T)$-section through the phase prism starting from a specific water-surfactant mixture and heading toward pure C_kMA suffices for identifying appropriate polymerizable microemulsions. Such a phase diagram for the systems under investigation here is schematically drawn in the context of the phase prism in Fig. 1 and as a single Cartesian phase diagram in Fig. 2. Similar phase diagrams for non-ionic surfactants can be found in [12].

Figure 2 shows a schematic representation of the two different two-phase regions and the channel of one-phase microemulsion between them. Two different effects on the interfacial film curvature can be seen from the schematic picture: (1) An increase in temperature makes the interfacial film curve around the oil domains.

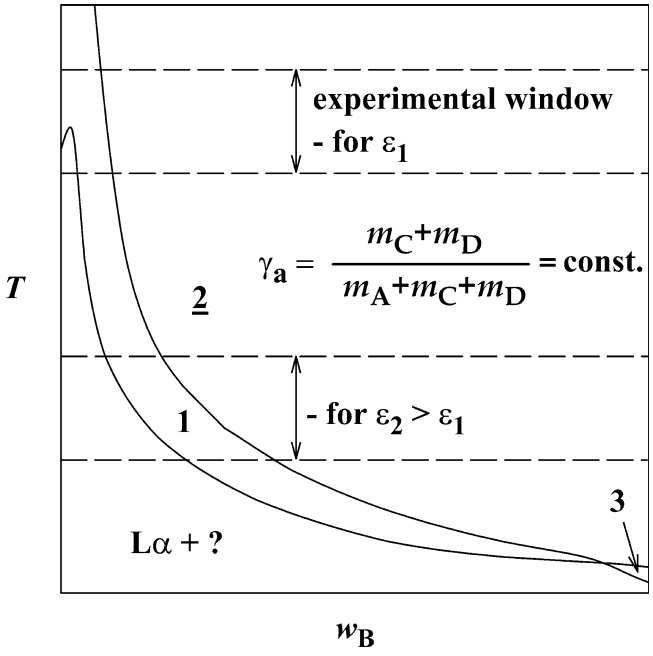

Fig. 2 One-phase microemulsion channel obtained from $w_B(T)$-section. Only certain parts of it can actually be recorded depending on salinity ε

Thus, a transition from the "Lα + ?" phase coexistence to a one-phase oil–water-microemulsion is found, and even a transition to a two-phase coexistence can be induced. In this work, we did not study the microstructure of the phase that coexists with the lamellar phase and, therefore, denote these coexistence regions as "Lα + ?". For a given amount of surfactant, the w_B of the emulsification-failure boundary decreases upon increasing temperature. Therefore, the best mutual solubility between water and oil occurs close to the balanced state, where three phases coexist. In practice, the actual curvature dependence on temperature is relatively weak, so for a given microemulsion system the one-phase channel in the $w_B(T)$-representation is steep and only a part of the whole one-phase channel can actually be measured within the temperature region accessible. (2) Upon increasing the salt concentration—while keeping it below the value for the balanced state determined by fish diagrams—the interfacial curvature decreases. This makes another temperature region accessible. For instance, one-phase regions of relatively hydrophilic systems (with a highly curved interface) will be found at lower temperatures after addition of salt. The two horizontal lines in Fig. 2 actually mean the lowest and highest practically applicable temperatures in experiment. The virtual temperature axis is therefore better understood in terms of an interfacial curvature axis, which for ionic surfactants increases with temperature but decreases with salinity.

Experimental section

Materials

Water employed was deionized and distilled twice. C_4MA and C_6MA were purchased from Scientific Polymer Products (Ontario, NY, USA) and used as received for phase behavior measurements but vacuum distilled to remove inhibitors prior to polymerization. AOT with purity >98% was from Fluka (Neu Ulm, Germany) and SDS with purity p.a. was from Sigma-Aldrich (St. Louis, MO, USA), both were used as received.

Phase diagrams

The ternary and quaternary mixtures were prepared by weighing sequentially water (or brine, respectively), oil and surfactant up to a total mass of about 2 g into a test tube with a magnetic stir bar. Phases present were determined visually in a water-bath at constant composition by varying the temperature. One-phase microemulsions and lamellar L_α phases are both transparent but can be distinguished by the birefringence of the L_α phase. Between these two phases, a coexistence region denoted as "L_α + μE" is present which was not investigated further. Two- and three-phase regions are both turbid and phase separation must be awaited.

For every pseudo-binary phase diagram at constant oil/(water + oil) volume ratio $\phi = 0.5$ the surfactant mass fraction γ was adjusted by titrating equal volumes of brine and oil. When recording $w_B(T)$-phase diagrams w_B was increased by adding oil to previously prepared mixtures.

Kinetics

A RC1 calorimeter (Mettler Toledo, Schwerzenbach, Switzerland) in isothermal operation mode was used for measuring the heat produced during the course of the polymerization. The head of the closed AP01 reactor was wrapped with heating cord and insulation to prevent periodic dripping of condensed water and monomer vapor to the reaction mixture. The reactor was initially filled with 700 g of the microemulsion and after achieving thermal equilibrium at 57 °C, the temperature was ramped to 62 °C to measure the heat capacity of the reactor contents. At 62 °C a precise amount of heat was applied to the reactor contents for calibration, after which the reactor was sparged with argon for 10 min and then sealed. The polymerization was initiated by injecting 1 ml of aqueous initiator solution. Upon completion of the reaction, the calibration and heat capacity measurement were repeated in reverse order.

The determination of conversion and heat of the reaction was performed with the standard RC1 software. The procedure for deoxygenating the microemulsion was followed to avoid pre-polymerization, minimize evaporation of monomer, and resulted in an optimal induction period (5–10 min) for the system to thermally equilibrate after the injection of initiator solution before the onset of polymerization.

Polymer characterization

Particle size and MWD of the polymer latexes were characterized using quasi-elastic light scattering (QLS) and size exclusion chromatography (SEC), respectively. To avoid multiple scattering and particle interaction during QLS analysis, the latexes were diluted with water prior to measurement at 25 °C. From the autocorrelation function the decay time was evaluated by using the cumulant method. Applying the Landau–Platzek together with the Stokes–Einstein relations, an apparent particle hydrodynamic radius was determined. The meaning of such a radius compared to a geometric radius yielded by electron microscopy has been discussed [6]. The hydrodynamic radius is slightly higher than the geometric radius and trends in sizes are reproduced correctly.

Size exclusion chromatography measurements were performed using non-shedding PL-Gel Mixed-A LS columns from Polymer Laboratories with a nominal fractionation range from 2×10^3 Da to 40×10^6 Da. Absolute molecular weight measurements were obtained using multi-angle laser light scattering (MALLS, Wyatt DAWN DSP) and differential refractive index (Waters R410) detectors. The very high molecular weights and low polydispersities of the microemulsion polymerized samples require high dilutions to avoid column overloading and/or apparent shear degradation. A flow rate of 0.5 ml/min was used and polymer concentrations as low as 5 ppm were found to be necessary. Reliable determination of the eluting concentration from the differential refractive index increment required the use of stabilized tetrahydrofuran (THF) for the mobile phase, precise above-ambient temperature control (40 °C), and long equilibration times (several hours).

SANS monomer partitioning measurements

For the equilibrium SANS swelling experiments, we followed the same experimental and data analysis procedures described previously [5]. Briefly, samples containing varying ratios of the polymerized microemulsions and original unpolymerized microemulsions were mixed in vials and transferred into 2 mm path length SANS cells. The SANS cells were made from stainless steel blocks with crystalline quartz windows sealed with PTFE coated silicone o-rings. The samples were allowed to equilibrate at 62 °C before SANS spectra were acquired.

Phase behavior: fish diagrams-$\gamma(T)$ sections

To assess the potential of AOT-based polymerizable microemulsions, the dependence of the efficiency and phase inversion temperature on the salinity was explored by systematically measuring fish-type phase diagrams. Without salt, the state of zero mean curvature state lies below accessible temperatures (0 °C). Thus, we start our phase behavior investigations from the well-known H_2O/NaCl–*n*-octane–AOT system with $\varepsilon = 0.008$. Progressive replacement of octane with C_6MA shifts the fish to higher temperatures. Systematically increasing the C_6MA fraction in the mixture while reducing ε to 0.003 yields the H_2O/NaCl–C_6MA–AOT phase diagram shown in Fig. 3.

Bis(2-ethylhexyl)sulfosuccinate is a highly efficient surfactant for microemulsifying C_kMA, i.e., only a very small amount of AOT ($\tilde{\gamma} = 0.024$) is necessary to generate a one-phase microemulsion containing equal volumes of water and C_6MA at $\tilde{T} = 45.0\,^{\circ}C$. The large, but thermodynamically stable, microstructures present in these highly efficient microemulsions give samples that appear cloudy but effectively transmit red light. A common difficulty in studying multiphasic samples of

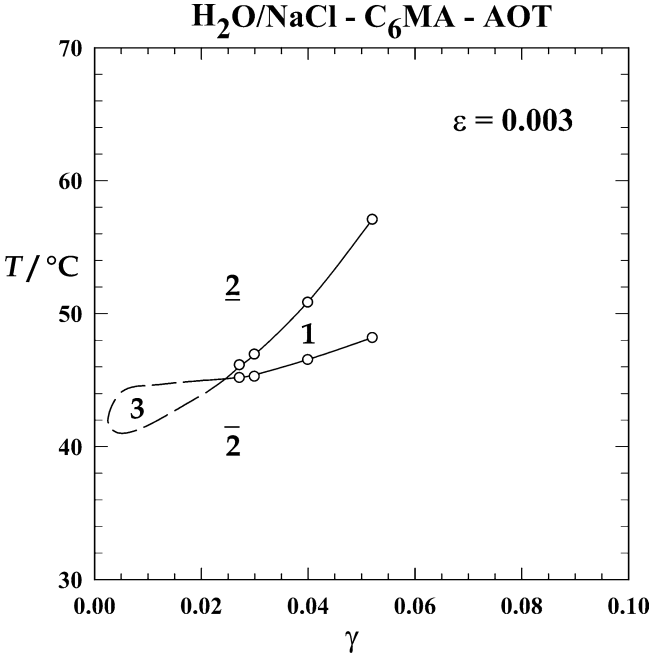

Fig. 3 Very efficient polymerizable microemulsions result when applying anionic AOT surfactant as shown by the fish diagram

surfactants that form efficient microemulsions is their slow phase separation. As there is actually no practical way to distinguish between two- and three-phase regions without awaiting complete phase separation, we were unable to determine precisely the three-phase region. A possible extension of the fish body—the three-phase coexistence region—is drawn in dotted lines to guide the eye.

To examine the effects of electrolyte concentration and C_kMA hydrophobicity, we recorded fish diagrams for C_4MA at three different values of ε (Fig. 4). A comparison of Figs. 3 and 4 reveals that upon decreasing k by 2 at constant $\varepsilon = 0.003$, $\tilde{T}$ increases ~23 K while the efficiency drops slightly. Decreasing ε in steps of $\Delta\varepsilon = 0.001$ causes a progressive reduction in $\tilde{T}$ and small changes in efficiency.

Phase behavior: $w_B(T)$ sections

After locating the balanced state for selected C_kMA microemulsions, we then proceeded to identify regions of the phase prism at varying oil to water ratios with the overall intent of finding suitable microemulsions for polymerization. While keeping all other variables constant, boundaries between one and two-phase regions were recorded as a function of the overall monomer weight fraction and temperature for one ternary and two quaternary mixtures. Starting with the basic system H_2O/NaCl–C_kMA–AOT/SDS the effects of tuning the interfacial curvature are demonstrated by systematically varying the tuning parameters: temperature, salt concentration, and ratio of AOT and SDS surfactants. The results of these phase behavior investigations are compiled in Fig. 5. The emulsification-failure and the Lα + ? one-phase transition boundaries are plotted with open and full symbols, respectively.

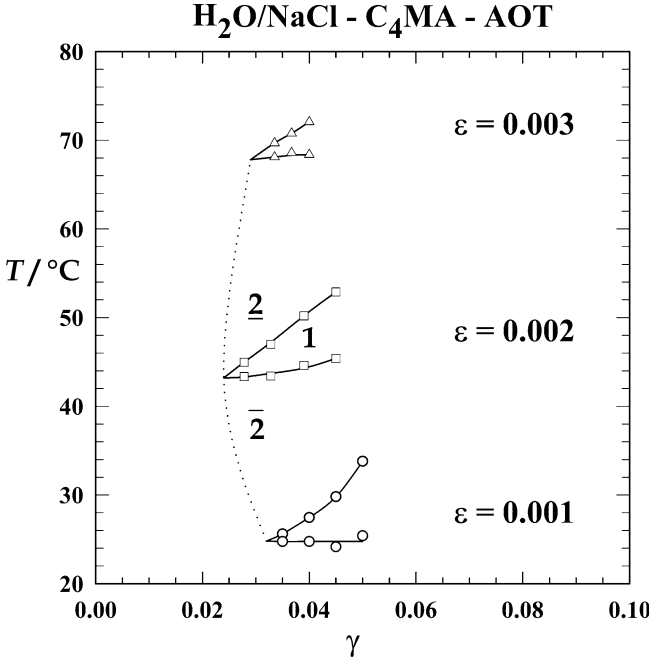

Fig. 4 Salinity dependence of the phase inversion. The phase inversion temperature increases upon increasing salinity

Effect of salt concentration

For mixtures H_2O/NaCl–C_6MA–AOT, four different $w_B(T)$-sections were recorded at constant $\gamma_a = 0.04$ and $\varepsilon = 0$, 0.001, 0.002, and 0.003 (Fig. 5a).

In this series, the interfacial curvature induced by the increasing salinity is expected to drop significantly. As shown in Fig. 5a, a change in ε can shift a large proportion of the one-phase channel to temperature regions suitable for polymerization. It is interesting to note that for the salt-less system the binary water-surfactant mixture is one-phase above 60 °C while all other channels start at low w_B with the two phases, Lα + ?.

Effect of surfactant concentration

For mixtures H_2O–C_6MA–AOT, three different $w_B(T)$-sections were recorded for constant $\varepsilon = 0$ and $\gamma_a = 0.04$, 0.07, and 0.10 (Fig. 5b). The sequence of one-phase channels resembles the one in Fig. 5a and from this, we infer that the interfacial curvature decreases with the surfactant concentration or more precisely with the surfactant-to-monomer-ratio. Changing ε from 0 to 0.002 while γ_a is fixed at 0.04 has approximately the same effect on the one-phase channel as an increase in γ_a from 0.04 to 0.10 (i.e., a factor of 2.5) at $\varepsilon = 0$.

Effect of the AOT/SDS ratio

Starting from the system with $\gamma_a = 0.10$, SDS was added progressively to yield three $w_B(T)$-sections (Fig. 5c) wherein the weight fraction of SDS in the surfactant mixture $\delta = m_{SDS}/(m_{SDS} + m_{AOT})$ was varied from $\delta = 0$ to 0.300. Addition of SDS increases the interfacial curvature and has the same effect as a decrease in either ε or γ_a.

Microemulsion polymerizations

All polymerizations were carried out at a fixed temperature of $T = 62$ °C. The initiator concentration was fixed at 0.1 wt% with respect to C_6MA to maintain a constant ratio ρ_0 between M_0 in Eq. 2. To emphasize the important relationship between phase behavior and

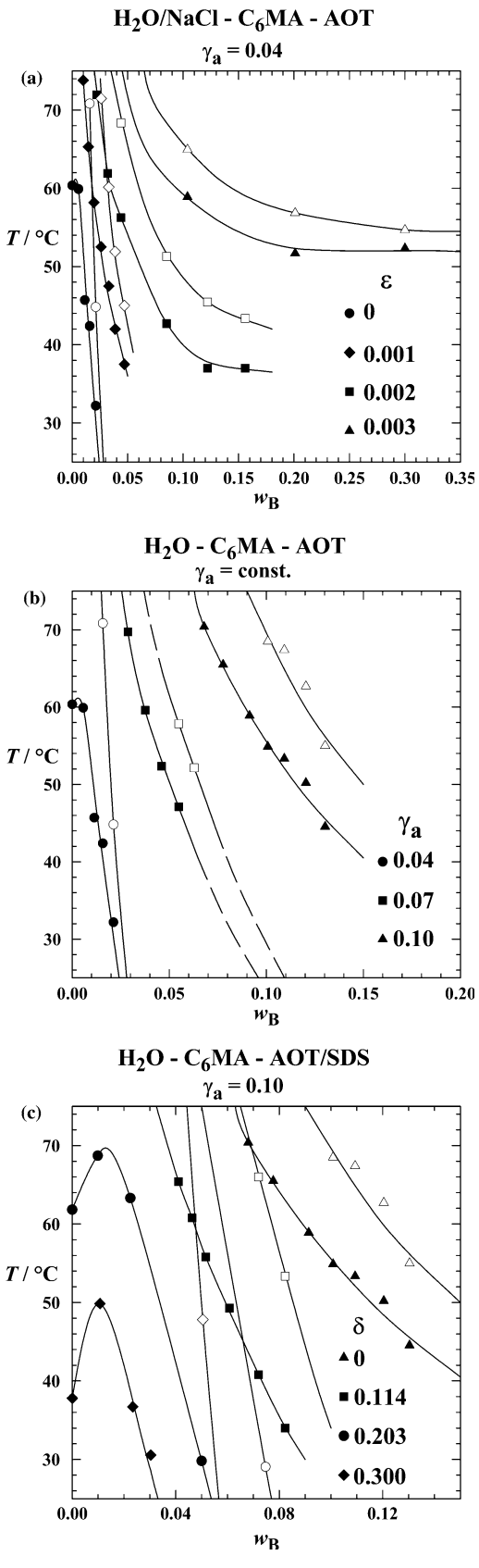

Fig. 5 $w_B(T)$-sections for variations of salinity (**a**), surfactant weight fraction (**b**), and cosurfactant weight fraction (**c**)

polymerization kinetics, the temperature dependent one-phase channels of Fig. 5 are re-plotted as isothermal phase diagrams in Figs. 6, 7 and 8 and shown next to the kinetic profiles of select microemulsions whose composition are denoted in the phase diagrams by full circles. For the ternary system H_2O–C_6MA–AOT only a portion of the isothermal Gibbs' phase triangle is shown in Fig. 7. The conversion f shown in the kinetic profiles refers to the calorimetric conversion which assumes full conversion at the end of the thermal signal. However, slight differences might occur if residuals of monomer do not convert to polymer, which for these reactions is assumed to be a minor effect.

The key assumption of the Morgan et al. [8] model that is expected to be most sensitive to changes in surfactant phase behavior is the assumption of a linear monomer concentration profile. Previous SANS studies of monomer partitioning between polymer particles and swollen-micelles confirm that this approximation is valid for a wide range of methacrylate and styrene polymerizations with droplet-type microemulsions of DTAB surfactant. Thus, we start our investigations of microemulsion polymerizations in AOT/SDS systems by first measuring the monomer partitioning profile.

For the single-phase H_2O–C_6MA–AOT/SDS microemulsions with $\delta = 30$ (Fig. 8), we performed SANS monomer partitioning measurements by measuring the SANS spectra of mixtures of the fully polymerized microemulsion with the original unpolymerized microemulsions replacing H_2O with D_2O. A detailed description and validation of this experimental technique together with the SANS data analysis procedures have been published previously [1, 5]. Briefly, the particle size distribution of the fully polymerized microemulsions is approximated by a Schultz distribution characterized by two globally fitted parameters: average radii and standard deviation. The number density and radii of particles in this distribution are then linearly and volumetrically scaled relative to the known mixing ratio and the model-fitted concentration of monomer in the polymer particles. Model SANS spectra are calculated using Vrij's equations [26] for polydisperse hard spheres and fitted to the experimental SANS spectra.

The quality of the data fitting is consistent with our previous experience. The SANS model fitted Schultz distribution of the unswollen fully polymerized latex has an average radii of 220 Å that is only slightly smaller than the measured hydrodynamic radii of 247 Å (Table 1). The corresponding monomer concentrations within the polymer particles over the course of polymerization obtained from fitting the SANS data are

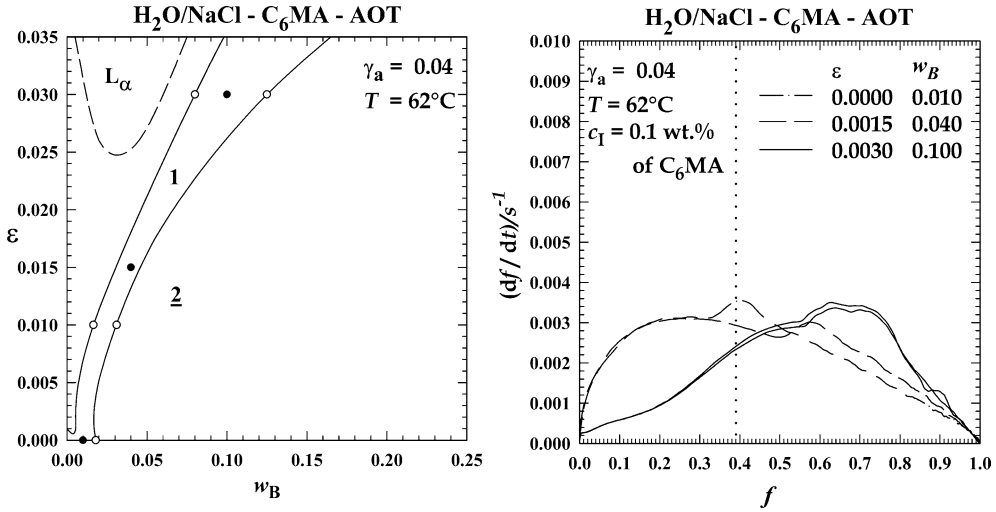

Fig. 6 Variation of phase behavior (*left*) and polymerization kinetics (*right*) on salinity at constant temperature and surfactant weight fraction. Good reproducibility can be seen from the two curves for different experiments with $\varepsilon = 0.0030$

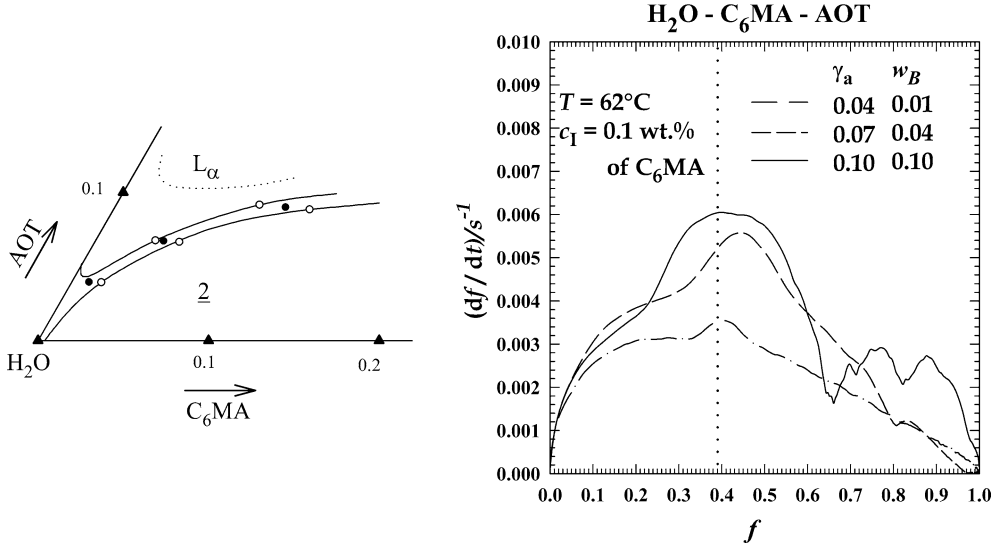

Fig. 7 Variation of phase behavior (*left*) and polymerization kinetics (*right*) on surfactant weight fraction at constant temperature

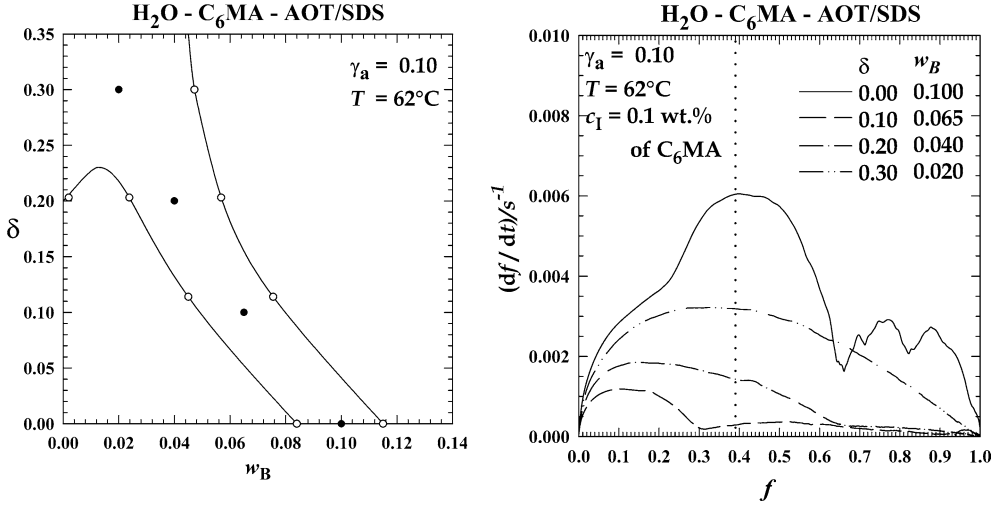

Fig. 8 Variation of phase behavior (*left*) and polymerization kinetics (*right*) on cosurfactant weight fraction at constant temperature

Table 1 Composition parameters together with results of particle size and molecular weight measurements for polymerization experiments

ε	γ_a	δ	w_B	r_H/nm	P.D.I.	$M_w/10^6$ g/mol	M_w/M_n
0	0.040	0	0.010	39.3	0.47	14.0	1.4
				1400	0.25		
0.0015	0.040	0	0.040	28.1	0.16	21.0	1.4
0.0030	0.040	0	0.100	38.7	0.31	30.0	1.5
0	0.040	0	0.010	39.3	0.47	14.0	1.4
				1400	0.25		
0	0.070	0	0.040	28.9	0.20	21.0	1.5
0	0.100	0	0.100	24.8	0.33	38.0	1.9
0	0.100	0	0.100	24.8	0.33	38.0	1.9
0	0.100	0.10	0.065	21.4	0.23	5.5	2.1
0	0.100	0.20	0.040	21.5	0.16	7.6	1.8
0	0.100	0.30	0.020	24.7	0.29	15.8	1.5

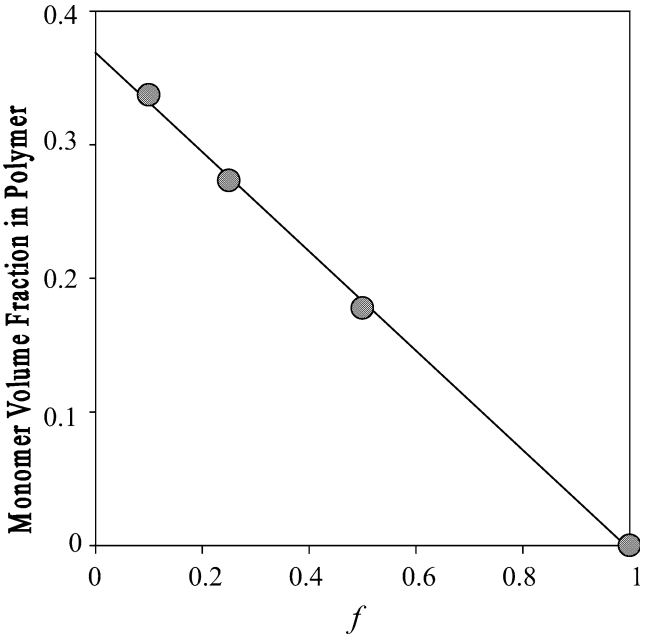

Fig. 9 Results of partitioning measurements by means of SANS

plotted in Fig. 9. The linearity of the monomer concentration profile is reminiscent of our previous measurements on C_6MA/DTAB microemulsions. The validity of this and other assumptions of the Morgan model altogether lead to a maximum rate of polymerization that is observed at ~39% conversion for AOT/SDS mixing ratio of $\delta = 30$ (Fig. 8).

For model systems of C_6MA, n-C_4MA, t-C_4MA, styrene with cationic DTAB and/or DDAB surfactants, wherein the initial microemulsion compositions were purposely chosen such that no-phase boundaries are crossed with decreasing monomer concentration, the polymerization rate increases rapidly to reach a maximum between 20% and 39% conversion. As mentioned earlier, systematic studies of variations in the maximum rate between 20% and 39% conversion have led to a good understanding of the effects of biradical termination, diffusional limitations, and slight non-linearities in monomer concentration profiles. Linearity of the monomer concentration profile, which arises from a progressive linear decrease in the chemical potential of the monomer over the course of polymerization, along with negligible biradical termination are the key assumptions of the Morgan model that we expect to be invalidated by phase separation and changes in interfatial film microstructure. Decoupling these phenomena by direct measurement of the monomer concentration profile and radical concentrations in phase separating or microstructurally changing systems has proven to be a challenging endeavor. Here, we present some of our findings that show clear and significant correlations between complex phase transitions and polymerization characteristics.

Effect of the SDS fraction δ and phase separation during polymerization

Starting from the base case of $\delta = 0.3$, which follows the kinetic profile predicted by the Morgan model, a slight decrease in SDS fraction to $\delta = 0.2$ leads to a significant decrease in polymerization rate and shift in a maximum rate of polymerization to ~15% conversion as shown in Fig. 8. A further decrease to $\delta = 0.1$ results in a further reduction in polymerization and shifts the maximum rate to ~10% conversion. The accompanying decrease in average molecular weight from 15.8 MDa to 5.5 MDa (Table 1) also indicates an increase in termination. It is apparent that the effects of incipient phase separation during polymerization influences the polymerization rate well before the phase boundary is actually crossed. For example, the AOT/SDS microemulsion which starts at $\delta = 0.2$ and $w_B = 0.04$ is expected to cross the phase boundary at $w_B = 0.024$ or at least after 40% conversion, ignoring the swelling of the polymer particles by monomer. However, the maximum rate is noticeably shifted from ~35% to ~15% conversion, much below the conversion at which phase separation is

expected to occur. This shift in the maximum rate that occurs before the phase boundary is reached is most likely associated with non-linearities in the monomer concentration profile that has been observed previously for styrene/DTAB microemulsion polymerizations that start close to the phase boundary [5]. Possible reasons for the increased rates of termination that would lead to the decrease in molecular weight in these systems include reduced compartmentalization caused by phase separation of monomer into micrometer sized surfactant-rich droplets or microstructural changes from swollen-micelles to larger surfactant structures over the course of polymerization, e.g. wormlike or cylindrical micelles. While plausible, these explanations are very difficult to prove. Nonetheless, we were very surprised by the sudden recovery in polymerization rate and molecular weight (up to 38 MDa) that occurs when no SDS is added ($\delta = 0$). The sudden enhancement in polymerization is also accompanied by complex but reproducible secondary features, e.g., maxima at ~75 and ~90% conversion that cannot be explained by the Morgan model. To probe deeper into the microstructural changes that drive this unexpected phenomena, we proceeded to further characterize the phase behavior and polymerization characteristics of AOT microemulsions containing no SDS.

Effect of microstructural changes to a lamellar phase

The phase behavior of the H_2O, C_6MA, AOT system containing no SDS is shown in Fig. 7. The microemulsion phase exists as a very narrow channel that is bound on the right side by a two-phase region that upon mixing forms oil in water emulsions and on the left side by a two-phase region wherein the microemulsion coexists with a lamellar phase. During polymerization, the complex mixture of remaining monomer, surfactant, and water in equilibrium with the polymer particles presumably forms this biphasic mixture of microemulsion in equilibrium with a lamellar phase.

The kinetic profiles (Fig. 7) and molecular weight data (Table 1), suggest that the presence of this lamellar phase enhances the rate of polymerization primarily through a reduction in termination rates. As the surfactant and monomer loadings are adjusted to navigate downward along the narrow microemulsion channel and to reduce the volume of lamellar phase formed during polymerization, we observe that the polymerization rate and molecular weights are reduced. Although the kinetic profile for the lowest surfactant concentration ($\gamma_a = 0.04$) still shows a sharp secondary maxima at ~40% conversion, these measurements indicate that the kinetic profile would revert back to the smooth profile with a single maxima at ~39% as predicted by the Morgan model if the formation of the lamellar phase can be completely suppressed. Polymerization in lamellar phases, especially at high conversions of surfactant-rich systems, e.g., $\gamma_a = 0.10$, wherein the surfactant planes are separated by distances much less than the free dimensions of the polymer chains may constrain the termination between radical ends of polymer chains to two dimensions. This potentially reduces the rate of termination and an enhancement in polymerization rate at high conversions akin to the well-known Tromsdorff gel effect, but caused instead by the reduced mobility of two dimensionally constrained radical chains.

To test these hypothesis further, we mapped out the phase behavior of H_2O, C_6MA, and AOT microemulsions containing only low concentrations of surfactant ($\gamma_a = 0.04$) but added salt to induce the formation of a lamellar phase (Fig. 6). As more salt is added, it is evident from the phase diagram that more of the lamellar phase will be formed during polymerization. The kinetic profiles show that increasing the tendency toward formation of this lamellar phase initially causes a shift in the sharp secondary maxima to ~60% conversion that is later followed by a dramatic shift in the primary maxima to ~70% conversion with indications of an earlier maxima at ~45% conversion. Accompanying these changes in the kinetic profiles is a progressive increase in average molecular weight from 14 MDa to 30 MDa. Altogether, these observations suggest once more that the formation of lamellar phase suppresses termination at high conversions. However, unlike the surfactant-rich system of Fig. 7 ($\gamma_a = 0.10$), multiple maxima at high conversions are not observed presumably due to the smaller volume of lamellar phase that can be formed from the reduced amount of surfactant.

Conclusions

We have examined the phase behavior of a pseudo-ternary ionic surfactant system (water + NaCl)–C_6MA–(AOT + SDS). The parameters, ε, a measure for the salinity, and δ, fraction of SDS in the mixture of the two ionic surfactants permit independent movement to shift the temperatures of the phase boundaries. Increasing ε shifts the phase body up in temperature while increasing δ shifts it down. Accordingly, the temperature at which one-phase microemulsions form can be set.

Very efficient polymerizable microemulsions result when the curvature of the surfactant film is carefully balanced. Close to the balance state of efficient microemulsions, lamellar phases exist either alone or in coexistence with other phases, e.g., the microemulsion or an excess oil or water phase.

While polymerizations in the one-phase microemulsion follows the usual well-understood kinetics, phase

separation or transitions into lamellar phase region during the polymerization process result in severe systematical changes of the kinetics, which were not well understood.

Acknowledgements Part of the material presented is based upon activities supported by Deutsche Forschungsgemeinschaft under grant STR 311/2-1. O.L. is grateful for a visiting scholarship of the University of Delaware.

References

1. de Vries R, Co CC, Kaler EW (2001) Macromolecules 34:3233
2. Candau F (1992) In: Paleos CM (ed) Polymerization in organized media. Gordon and Breach Science Publishers, Philadelphia, pp 215–282
3. Antonietti M, Basten R, Lohmann S (1995) Macromol Chem Phys 196:441
4. Desai SD, Gordon RD, Gronda AM, Cussler EL (1996) Curr Opin Colloid Interface Sci 1:519
5. Co CC, de Vries R, Kaler EW (2001) Macromolecules 34:3224
6. Co CC, Cotts P, Burauer S, de Vries R, Kaler EW (2001) Macromolecules 34:3245
7. Lusvardi KM, Schubert K-V, Kaler EW (1995) Langmuir 11:4728
8. Morgan JD, Lusvardi KM, Kaler EW (1997) Macromolecules 30:1897
9. Morgan JD, Kaler EW (1998) Macromolecules 31:3197
10. Co CC, Kaler EW (1998) Macromolecules 31:3203
11. Co CC, de Vries R, Kaler EW (2001) In: Texter J (ed) Reactions and synthesis in surfactant systems. Proc Natl Acad Sci
12. Lade O, Beizai K, Sottmann T, Strey R (2000) Langmuir 16:4122
13. Strey R (1994) Colloid Polym Sci 272:1005
14. Kunieda H, Shinoda KJ (1973) Colloid Interface Sci 42:381
15. Shinoda K, Kunieda HJ (1982) Dispersion Sci Technol 3:233
16. Kahlweit M, Strey R, Firman P, Haase D, Jen J, Schomäcker R (1988) Langmuir 4:499
17. Schubert KV, Kaler EW (1996) Ber Bunsenges Phys Chem 100:190
18. Glatter O, Strey R, Schubert KV, Kaler EW (1996) Ber Bunsenges Phys Chem 100:323
19. Langevin D (1996) Ber Bunsenges Phys Chem 100:323
20. Lindman B, Olsson U (1996) Ber Bunsenges Phys Chem 100:344
21. Talmon Y (1996) Ber Bunsenges Phys Chem 100:364
22. Gradzielski M, Langevin D, Farago B (1996) Phys Rev E 53:3900
23. Kahlweit M, Strey R (1985) Angew Chem Int Ed Engl 24:654
24. Kahlweit M, Strey R, Schomäcker R, Haase D (1989) Langmuir 5:306
25. Maugey M, Bellocq A-M (1999) Langmuir 15:8602
26. Vrij A (1979) J Chem Phys 71:3267